JOURNAL OF SPACECRAFT AND ROCKETS
Vol. 35, No. 3, May–June 1998

Hybrid Euler/Particle Approach for Continuum/Rarefied Flows

Roberto Roveda,* David B. Goldstein,† and Philip L. Varghese‡
University of Texas at Austin, Austin, Texas 78712-1085

A single computational technique that couples Nadiga's four-speed adaptive discrete velocity Euler solver with Bird's direct simulation Monte Carlo method has been implemented to model mixed rarefied and continuum flow simultaneously. The process of interaction between the continuum and particle domains relies on the continuous exchange of properties at a common boundary. The novel application of ghost cells decreases the statistical noise of the direct simulation Monte Carlo property signal along the interface. The hybrid code employs the direct simulation Monte Carlo method to simulate disconnected patches embedded within a continuum flow. These patches can be moved and deformed adaptively on a single grid to track nonequilibrium regions of the flow. Numerical results are presented for the adaptive simulation of a one-dimensional shock tube and for the nonadaptive calculation of unsteady two-dimensional pressure-driven slit flow impinging on a target plate. The hybrid, adaptive shock tube simulation demonstrates the stability of the interface and the capability of the adaptive algorithm to capture physical phenomena such as shock waves, expansion waves, and contact discontinuities. The simulation of slit flow presents a simplified rendition of a nozzle plume striking a spacecraft surface. The test cases presented provide stepping stones to more complex two- and three-dimensional hybrid, adaptive flow simulations.

Nomenclature

Kn	= global Knudsen number, λ_∞/L
Kn_{GLL}	= gradient-length local Knudsen number
k	= Boltzmann's constant
L	= characteristic length
m	= molecular mass
n	= number of direct simulation Monte Carlo method (DSMC) ghost levels
n_m	= number of DSMC simulated particles in a cell
P_B	= Bird's breakdown parameter
T	= translational temperature
T_{sample}	= instantaneous temperature from DSMC sample
t	= time
u	= total component of velocity in x direction, $u' + \bar{u}$
u'	= thermal component of velocity in x direction
$\bar{u}$	= mean component of velocity in x direction
z	= normally distributed variable
Δf	= temperature correction factor
λ	= mean free path
ν	= DSMC collision frequency
$\boldsymbol{\xi}$	= mean of normal probability density distribution
ρ	= macroscopic density
ρ_N	= normalized density gradient
σ_2	= variance of normal probability density distribution

Subscripts

d	= shock-tube driven section
i	= integer index
w	= wall
x, y	= Cartesian coordinate axes
∞	= freestream or initial low-pressure reservoir conditions
1	= upstream, shock-tube driven section
2	= downstream, shock-tube driver section

Received May 29, 1997; revision received Nov. 21, 1997; accepted for publication Dec. 9, 1997.

*Graduate Research Assistant, Department of Aerospace Engineering and Engineering Mechanics. E-mail: roberto@cfdlab.ae.utexas.edu. Student Member AIAA.

†Assistant Professor, Department of Aerospace Engineering and Engineering Mechanics. Senior Member AIAA.

‡Professor, Department of Aerospace Engineering and Engineering Mechanics. Senior Member AIAA.

Introduction

THE accurate prediction of aerodynamic and thermodynamic loads on vehicles that operate in the transitional flow regime motivates the development of more accurate and efficient computational methods than are currently being used. The goal of the present study is to combine the efficiency of an Euler equations solver in the continuum region with the accuracy of the direct simulation Monte Carlo method (DSMC) in nonequilibrium flow areas. Finite difference discretization of the Euler equations[1,2] and particle-based methods (DSMC[3,4]) often cannot adequately model near-continuum flows when they are applied separately. Although computationally efficient to solve, the Euler equations neglect departures from equilibrium due to momentum and thermal and mass diffusion and are invalid in regions of strong nonequilibrium. The DSMC approach performs well in modeling flows having low density or small characteristic flow dimensions but becomes less computationally efficient as the flow progresses from free molecular, through transitional, to continuum.

The new, coupled continuum-particle technique offers the following contributions: 1) analysis of unsteady flows is possible because information is exchanged at every time step and because moving DSMC patches can track traveling waves; 2) the novel application of ghost cells is described to minimize the noise in DSMC interface properties without resorting to DSMC ensemble averaging; 3) the employment of adaptive DSMC patches to resolve areas of nonequilibrium improves the accuracy of the solution and maintains reasonable computational cost; 4) the lack of oscillations or extraneous waves (except for DSMC noise) propagating from the DSMC/Euler interface shows that the procedure is stable; and 5) the procedure to exchange information at the interface provides suitable boundary conditions for subsonic outflow in DSMC.

The objective of this work is to develop a hybrid code whose results will enhance the understanding of nozzle plume flows and accurately predict plume surface impingement loads. Specifically, the method will eventually be applied to analyze the structure of Space Shuttle maneuvering thruster plumes.[5,6]

Literature Review

Previous efforts have employed continuum and particle methods in uncoupled,[5,7] weakly coupled,[8] and strongly coupled[9,10] fashions. Uncoupled approaches implement a unidirectional flow of information: from continuum to the particle method (DSMC). Particles generated according to the continuum fluxes at a fixed interface travel into the DSMC region. Weak coupling techniques periodically update the continuum solution through the use of the interface fluxes or properties obtained from DSMC, whereas strongly

coupled methods increase the frequency of information exchange. These approaches produce a physically correct solution of complex steady flows by resolving nonequilibrium areas with a particle method. However, the fixed boundary may result in the superfluous application of DSMC in equilibrium areas. More importantly, the ensemble averaging of DSMC interface information precludes the placement of DSMC patches to track and resolve shock, expansion, and shear waves that may propagate throughout unsteady flows.

Type of Interface

The existing continuum-particle coupling methods implement variations of a basic scheme: property extrapolation to generate interface fluxes. That is, the continuum approach updates its cell-centered properties using half fluxes or net fluxes at the interface as boundary conditions. In the other direction, continuum macroscopic interface properties and fluxes are used to specify the distribution function of entering particles.

Hash and Hassan[8] studied the solution of planar Couette flow with a hybrid Navier–Stokes–DSMC solver to test the validity of two coupling methods: the Marshak conditions[11] and the extrapolation of flow properties. The authors discarded a third flux extrapolation method because of excessive statistical noise associated with the higher velocity moments used to calculate the required DSMC shear stress and heat flux. The Marshak condition was used to obtain the net interface flux as a sum of the DSMC and Navier–Stokes half fluxes. DSMC half fluxes were evaluated by counting the number of particles crossing the interface, whereas the explicit equations in terms of macroscopic properties provided the Navier–Stokes half fluxes at the interface. The second method extrapolated properties from the center of boundary cells to the interface and performed an iterative procedure until the values from the continuum and particle techniques agreed on both sides of the interface. Simulations with an increasing number of particles and at a higher coupling frequency between the continuum and rarefied regions revealed that the Marshak conditions seemed to provide the most accuracy and efficiency when compared with the pure DSMC calculation. More recently, however, Hash and Hassan[12] showed that the high statistical scatter exhibited by the DSMC half fluxes precluded the application of the Marshak conditions to low-Mach-number flow regions.

Wadsworth and Erwin[9,10] carried out simulations of one-dimensional shock waves and two-dimensional slit flows using a cell-centered flux matching interface formulation. In the cell-centered technique, the cumulative sampled value of DSMC cell-centered conserved quantities adjacent to the interface provided the boundary condition to integrate the Navier–Stokes equations in the continuum region. The flux into the DSMC region was calculated by interpolation to the interface of the cell-centered Navier–Stokes solution. Thus the coupling was not strictly time accurate but improved as steady-state conditions were approached.

The Marshak[11] and the flux matching[9,10] techniques represent interesting steps toward a generally useful hybrid approach. However, no attempts appear to have been made to solve unsteady flows or to decompose the domain adaptively according to the degree of local translational equilibrium.

Location of Interface

The gradient-length local Knudsen number[3] Kn_{GLL} and Bird's breakdown parameter[13] P_B embody the physical and numerical criteria that identify the boundary between continuum and rarefied computational domains. Physically, the Knudsen number measures the departure of the local translational distribution function from the equilibrium state. The term P_B represents a correlation parameter that indicates departure from equilibrium in flows containing expansion waves.

Numerically, it is generally thought that continuum methods do not provide an accurate description of flows when the global Knudsen number

$$Kn = \lambda_\infty / L \tag{1}$$

based on a characteristic length L increases above about 0.1 (Ref. 3). However, the gradient-length local Knudsen number (presented here in steady one-dimensional form),

$$Kn_{\mathrm{GLL}} = \frac{\lambda_x}{\rho}\left|\frac{\mathrm{d}\rho}{\mathrm{d}x}\right| \tag{2}$$

based on the local density gradient, predicts the breakdown of continuum approaches in local nonequilibrium flow regions better than the global Knudsen number. Similarly, Bird's study of expanding flows indicates failure of the continuum approach as P_B (shown here in steady one-dimensional form),

$$P_B = \frac{1}{\rho v}\left|\bar{u}\frac{\mathrm{d}\rho}{\mathrm{d}x}\right| \tag{3}$$

increases above 0.05 (Ref. 13).

Boyd et al.[14] conducted an investigation to assess the validity of density-based Kn_{GLL} and P_B as failure thresholds of the Navier–Stokes solution in transitional hypersonic flows. The authors accurately quantified the density-based Kn_{GLL} and P_B within one-dimensional normal and two-dimensional bow shock waves for full continuum and full particle calculations. Both solutions were deemed valid if they agreed within 5%, whereas a larger discrepancy indicated that the Navier–Stokes approach had failed. Their results indicated that translational nonequilibrium may exist for $Kn_{\mathrm{GLL}} > 0.05$. A more conservative estimate should be adopted in general because DSMC noise and unsteady effects do not allow a precise positioning of the interface.

In a study aimed at resolving regions of translational nonequilibrium with DSMC, Wadsworth and Erwin[9] stretched the Navier–Stokes domain beyond its region of assumed global validity as they positioned interfaces at points successively closer to the center of a one-dimensional shock. They suggested using the magnitude of the integrated differences between the local and equilibrium velocity distribution functions to gauge the validity of the particle method at a particular point in the flow. However, the computational costs of this adaptive procedure are large due to the number of particles required for a smooth, integrable distribution function and also because of the integration in a two- or three-dimensional phase space. The hybrid profiles maintained good qualitative agreement with full DSMC baseline calculations, despite the presence of coupling points within the nonequilibrium region. Nonetheless, even if accuracy was maintained for the specific case of a standing shock wave, it is desirable to position the interfaces conservatively in the general case.

Present Approach

We chose to interface Nadiga's adaptive discrete velocity (ADV) method[15–17] with Bird's DSMC.[3,4] ADV is a kinetic theory approach that integrates the Euler equations for a 27-discrete-velocity (4-speed) gas model through the use of a flux-splitting/total variation diminishing scheme based on Nadiga and Pullin's flux-splitting equilibrium method.[17] The ADV approach assumes an equilibrium distribution function based on macroscopic properties at each cell center but retains a nonequilibrium distribution function at cell boundaries because of the superposition of distinct cell-centered fluxes from neighboring cells. The combination of a fast quasiparticle approach (ADV) with a true particle simulation (DSMC) creates an efficient coupling between continuum and rarefied regions.

Type of Interface

Interface Information Exchange

Figure 1 illustrates the strong mechanism of information exchange that occurs in both directions between the continuum and rarefied computational domains. The hybrid technique decouples the calculation into an ADV and a DSMC step.

In the continuum region, the ADV Euler solver determines the interface continuum fluxes through the use of DSMC macroscopic properties. The three DSMC cells adjacent to the interface are treated as an extension of the ADV domain, and the macroscopic DSMC properties therein are used to obtain DSMC-to-ADV fluxes necessary for finite volume integration. The detailed explanation of the ADV interface calculations will be given later. DSMC evaluates the density ρ, the velocity vector $\boldsymbol{V}$, and the specific internal energy e through a simple, fast averaging procedure that obviates the need for statistically noisy and computationally expensive particle

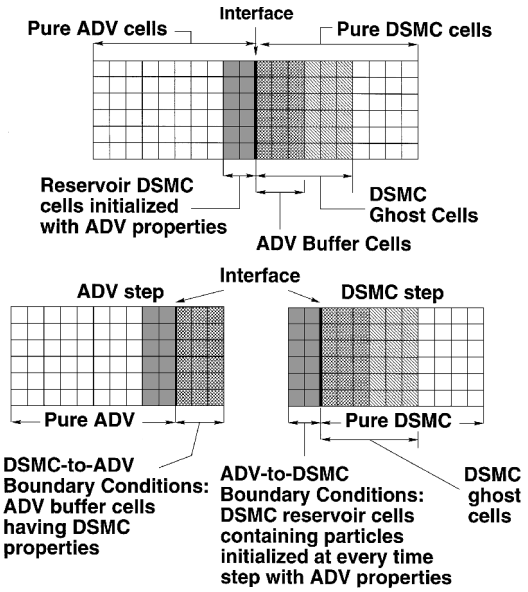

Fig. 1 ADV–DSMC interface cell sets.

counting routines to generate fluxes. The statistical noise of DSMC boundary properties may also be decreased considerably by the application of smoothing ghost cells. Interpolation of the properties to the interface and generation of the ADV buffer cell half fluxes becomes completely internal to ADV and ensures conservation of mass, momentum, and energy at the interface.

In the opposite direction particles travel into the DSMC domain from a layer of two ADV cells disguised as particle reservoir cells. A later section describes the detailed procedure that initializes the thermal velocities and positions of the reservoir particles. Tests on shock waves at high Mach numbers revealed that for a reasonable time step a negligible number of high-speed particles will travel farther than two cells.

Effect of Statistical Fluctuations on Temperature

It was observed that sampling from a small number of DSMC particles consistently depresses the value of the translational temperature. Bird[3] attributes the depression effect to fluctuations that cause spurious velocities in a stationary gas (also see Ref. 18 for a discussion of Monte Carlo bias). Therefore, a correction factor is needed when evaluating the temperature from a finite sample of DSMC simulated molecules when the sample size decreases below about 100 particles.

The calculations presented employ an empirical inflation correction factor that is applied to the DSMC cells that contain fewer than 4000 simulated particles. The inflation correction Δf is determined a priori as the ratio of the instantaneous temperature values sampled from n_m molecules in equilibrium and the true value of the translational temperature. The number of simulated molecules in a DSMC cell (n_m) is then used to access the appropriate value of Δf and to correct the instantaneous value of the temperature:

$$T = T_{\text{sample}} \cdot [\Delta f(n_m)] \tag{4}$$

The correction is used to evaluate macroscopic properties in the ADV buffer cells, to generate macroscopic properties in ADV cells that spawn from ghost or real DSMC cells during the regridding process, and to correct output DSMC properties.

Further investigation of the temperature depression phenomenon produced an exact mathematical form of the DSMC-sampled temperature correction factor. To clarify this, examine the formula used for the translational temperature term in the x direction:

$$(k/m)T_x = \overline{u'^2} = \overline{u^2} - \bar{u}^2 \tag{5}$$

Consider the correspondence between a set of l simulated particle velocities $(u_i, i = 1, 2, 3, \ldots, l)$ and a finite sample of l observations $(z_i, i = 1, 2, 3, \ldots, l)$ distributed according to the normal distribution $f(z)$:

$$f(z) = (1/\sigma\sqrt{2\pi}) \exp[-(1/2\sigma^2)(z - \xi)^2], \qquad -\infty < z < \infty \tag{6}$$

If $(k/m)T_x$ is interpreted as the variance (σ^2) of the normal distribution in Eq. (6), then there is an exact analogy between Eq. (5) and the statistical problem of estimating the variance of the finite sample of observations normally distributed in accordance with Eq. (6).

It can then be shown[19] that Eq. (5) requires a correction factor for the proper evaluation of the temperature:

$$(k/m)T_x = [n_m/(n_m - 1)](\overline{u^2} - \bar{u}^2) \tag{7}$$

Steady DSMC calculations attain adequate sample size through the use of ensemble time averaging that drives the factor $n_m/(n_m - 1)$ to unity. In these cases, Eq. (5) is a good approximation for the estimation of the temperature. However, unsteady calculations that employ fewer than 100 particles per cell may experience a reduction in the translational temperature of 5% or more because the factor $n_m/(n_m - 1)$ increases significantly above unity as n_m decreases.

The exact correction of Eq. (7) explains the validity of the empirical correction factor in the calculations presented and will replace the empirical adjustment in all future hybrid calculations.

Generation of Reservoir DSMC Particles

To provide DSMC with boundary conditions, the algorithm generates the thermal velocities and initial positions of incoming DSMC particles from the ADV domain. Cell-centered density values in the two ADV cells adjacent to the interface (DSMC reservoir cells in Fig. 1) determine the number of reservoir DSMC particles to initialize. For each reservoir cell the algorithm generates the particle velocities from the equilibrium (Maxwell–Boltzmann) velocity distribution function that reflects the reservoir cell (ADV) macroscopic properties. The current hybrid method randomly distributes the DSMC particles within the reservoir cells as opposed to the common approach of positioning them on the coupling boundary. Particles that end their movement phase within pure DSMC regions are retained: Those that do not enter the DSMC domain are deleted. The same DSMC subroutine moves both DSMC and reservoir DSMC particles with a uniform time step.

Many particles must be generated. To expedite the generation of particles, the RF(0) subroutine suggested by Bird[3] was used to generate 12 lookup tables of 50,000 random numbers each. Such multiple independent tables counteract false nonequilibrium effects between temperature components caused by the use of sequential, nondistinct random fractions.[3] One set of five tables contains a normalized Gaussian distribution function used to initialize the particle velocity components. A second set of five tables contain uniformly distributed random numbers between -0.5 and 0.5 for use in the collision partner selection process and to randomly position particles. The generation of random coordinates occurs when creating DSMC particles in the pure and ghost DSMC cells (initially and during the regridding procedure) as well as positioning them in the reservoir cells. Two tables contain uniformly distributed integers between 1 and 5 that function as pointers to the velocity and position tables. A reasonably random sequence of numbers may be generated by occasionally hashing the pointer tables only. The sacrifice of memory space to store the random number table avoids repeated computationally intensive calls to the random number generator.

The reservoir cell procedure is fast and easy to implement and generates the DSMC fluxes through the interface in a natural way.

Ghost Cells

DSMC provides ADV with property values whose rms noise is proportional to the inverse square root of the number of simulated DSMC particles that generate the values. A simple increase in DSMC particles throughout the domain achieves rms noise reduction of DSMC properties but at unacceptable computational cost. However, providing a localized increase in the number of particles

through the use of ghost cells near the interface provides adequate smoothing without undue computational cost.

An n-parallel DSMC move-collide cycle occurs in a frame of n overlapping DSMC ghost levels that surround each DSMC patch and interact with ADV (Fig. 2). The ensemble average of the n relatively independent solutions (see later discussion) yields smoother ADV boundary conditions. Hence, we may compute with 40 particles per cell in most of a DSMC region, whereas, with 3 levels of ghost cells ($n = 3$), the ADV buffer cells see a random noise level closer to that found with 160 (3 ghost levels + 1 real level) particles per cell.

Figure 3 illustrates five possible events as particles travel through the ghost region. Particles entering the ghost region from DSMC reservoir cells (event 1 in Fig. 3) or from the interior of the DSMC domain (event 3) are cloned n times with each clone being distributed to a different ghost level. To ensure conservation of mass flux into the interior of the DSMC patches, those particles departing for the ordinary DSMC side from any one of the ghost levels (event 5) are destroyed with probability $n/(n+1)$. Particles that leave from any level for the ADV side (event 4) are lost altogether. Direct interlevel particle movement never occurs.

Ghost levels do not provide truly independent solutions because incoming particles are cloned exactly in events of type 1 and 3. Cloning particles destroys the true statistical independence of the n-ghost levels and only results in a partial decrease of statistical noise. Sufficient ghost zone width, however, provides n nearly independent realizations because particles lose their cloned identity by undergoing several independent collisions during travel through each ghost level.

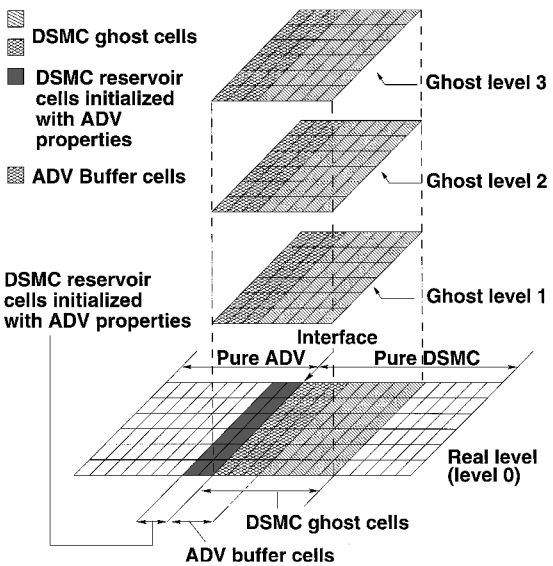

Fig. 2 Ghost level structure illustrating three ghost levels.

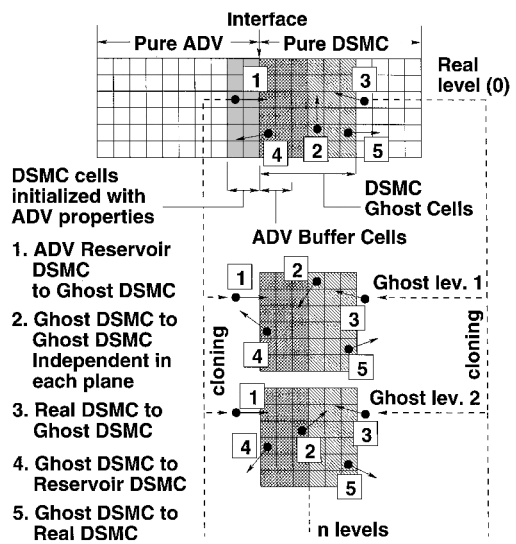

Fig. 3 Ghost level particle movement.

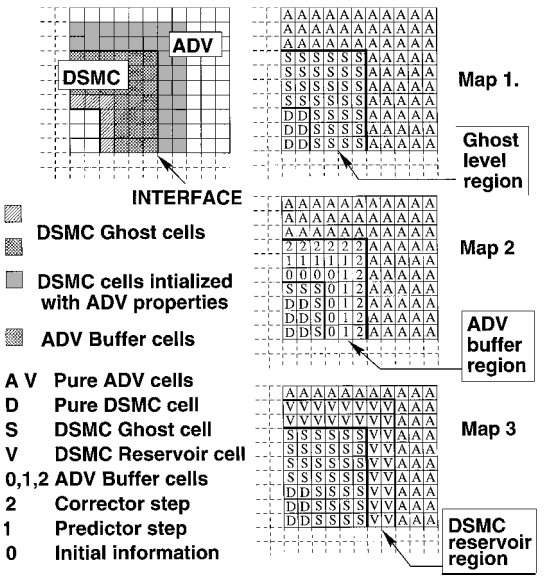

Fig. 4 ADV–DSMC ASCII map sets.

Programming Approach: Maps

The hybrid Cartesian grid is represented with ASCII character maps that describe the nature of a cell. This allows easy manipulation as well as contouring of DSMC patches to model bodies immersed in the flow. Three different maps specify the nature of the cells, depending on the task performed (Fig. 4).

Map 1 specifies whether the cell is a regular DSMC cell (D), ghost DSMC cell (S), or ADV (A). Map 2 distinguishes the ADV buffer cells (0, 1, or 2) that provide ADV with boundary properties from the DSMC domain. The predictor half step uses properties in cells of character 0 to update cells of character 1, 2, and A. The corrector half step utilizes the properties in cells of character 1 to update cells of character 2 and A. Through the creation of the interface discrete velocity distribution function, the corrector step generates the ADV interface half fluxes. Notice that the ADV buffer cells may be either ghost DSMC cells (S) or regular DSMC cells (D) if ghost smoothing is turned off ($n = 0$ in which case ghost DSMC cells transform to regular DSMC cells in map 1 as well). Map 3 characterizes the DSMC reservoir cells (V). Rapid characterization of cells by sweeping through the map allows fast application of the appropriate particle or continuum subroutine.

The preceding procedure allows rapid repositioning and modification of the DSMC regions using the adaptive grid procedure described in a later section. Calculations are then advanced in time based on the new grid.

Frequency of Coupling

ADV and DSMC are coupled to exchange property information within every calculation cycle. This strong coupling reduces variation of the properties on either side of the interface, obviating the need to reconcile such properties using computationally expensive iterative procedures. The appropriate time step synchronizes the information exchange between the DSMC (move-collide sequence) and ADV (predictor-corrector operation) cycles. The collision frequency limits the DSMC time step: particles should travel sub-mean-free-path distance during Δt. The continuum flow calculation faces the Courant–Friedrichs–Lewy constraint. However, the more stringent DSMC condition dictates the current choice of uniform time step throughout both continuum and particle regions. Variable time step may be implemented in the future once the validity of the interface coupling procedure has been thoroughly tested.

Location of the Interface

The present coupled technique adaptively positions the interface between DSMC and the continuum method into a region of mutual

validity where the effects of viscosity and heat conduction are negligible. The automatic processes of interface positioning can occur at every time step. The present hybrid method places the interface conservatively because the technique employs an ADV Euler solver instead of a Navier–Stokes solver and because of the uncertainty associated with the high noise levels accompanying unsteady computations.

Placement of DSMC Patches

A simple, inexpensive running-average low-pass filter employing a variable stencil width provides a smoothed density and velocity field. Note that the smoothed field does not affect the property integration; it serves only as a regridding tool. The term Kn_{GLL} [Eq. (2)], P_B [Eq. (3)], and the normalized density gradient,

$$\rho_N = \frac{\lambda_\infty}{\rho}\left|\frac{\mathrm{d}\rho}{\mathrm{d}x}\right| \tag{8}$$

based on the smoothed velocity and density fields determine the range of validity for each method. The Kn_{GLL} and P_B profiles by themselves identify only the nonequilibrium region that results from the temperature shock ahead of a shock wave,[14] whereas ρ_N extends the downstream coupling boundary well beyond the density shock.

Three cutoff parameters are evaluated for the weakest compression wave that we wish the DSMC patches to track. Because the width of the nonequilibrium regions grows progressively thinner as the Mach number increases, choosing cutoff values of Kn_{GLL}, P_B, and ρ_N that bracket a weak compression wave automatically guarantees the adequate capture of stronger shock waves. Figure 5 illustrates cutoff parameters for an instantaneous DSMC realization of a Mach 1.2 shock wave. The lowest cutoff among the upstream and downstream values that exceed the residual DSMC noise on either side of the wave are selected for each parameter. In this example the cutoff values correspond to $Kn_{\mathrm{GLL}} = 0.0010$, $\rho_N = 0.0013$, and $P_B = 0.0004$. DSMC is employed where any of the three parameters exceeds the values obtained from the preceding bracketing of a weak wave.

The artificially widened shock region that results from the filtered property gradients ensures that ADV is restricted to equilibrium flow and that DSMC patches completely envelop flow gradients. Figure 6 illustrates a sample regridding procedure in which the hybrid simulation of a traveling Mach 5.2 shock wave initially employs a pure DSMC domain. After regridding, DSMC is to be applied where one or more of the regridding parameters exceed the values selected in Fig. 5 (the region delineated by vertical lines in Fig. 6). ADV will simulate the remainder of the domain.

The cutoff value of the regridding parameters depends on the number of smoothing passes and the width of the smoothing region that contribute to the moving average of the velocity and density fields. The preceding parameters, although adequate for present purposes, may be slightly altered if the regridding procedure captures simulated patches with excessive DSMC noise. Hence, future research will attempt to provide more precise parameter cutoff values that will improve capture of compression and expansion waves and contact discontinuities of various strengths and in multiple dimensions.

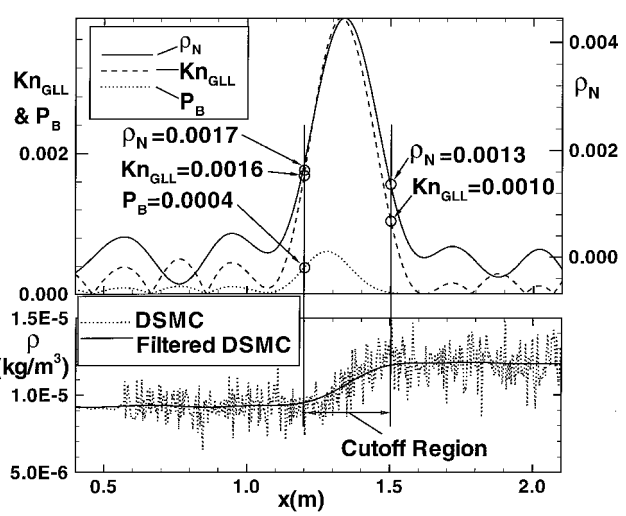

Fig. 5 Mach 1.2 shock wave cutoff region.

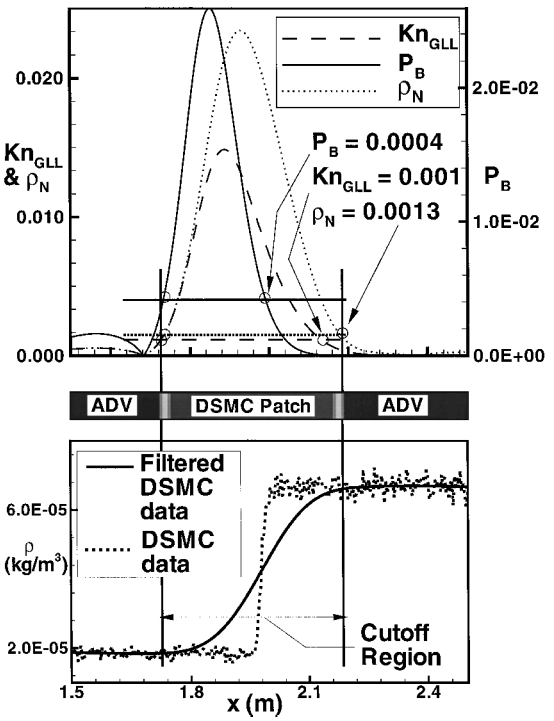

Fig. 6 Mach 5.2 shock wave DSMC patch location using cutoff parameters illustrated in Fig. 5.

Adaptive Boundary Location

The current technique reshapes and repositions DSMC patches periodically so as to track high-gradient, unsteady phenomena such as shocks, expansions, shear waves, and boundary layers. In the adaptive calculations that follow, a regridding interval of 5 to 10 time steps proved suitable to track unsteady wave patterns in supersonic flows.

As discussed earlier, the regridding procedure uses Kn_{GLL}, P_B, and ρ_N cutoff values to determine whether a cell changes its character from ADV to DSMC or vice versa. At first only pure ADV and pure DSMC cells are identified. If a cell is to switch from real or ghost DSMC to ADV, sampling the DSMC particles generates ADV macroscopic properties. All ghost and pure DSMC particles in that cell are then removed from the DSMC array. Conversely, if the switch from ADV to DSMC occurs, DSMC particles are initialized from the ADV macroscopic properties and randomly positioned throughout the new DSMC cell.

A further sweep then identifies the DSMC–ADV interface and changes the character of boundary cells to create the appropriate frame of ghost cells, reservoir DSMC cells, and ADV buffer cells. The algorithm assigns ghost cells according to a predetermined depth. Turning regular DSMC to ghost DSMC cells requires cloning the regular cells through the n ghost levels.

Results

The hybrid ADV–DSMC technique has been successfully applied to analyze simple configurations of standing and moving one-dimensional shocks, expansion waves, a propagating shear layer, and the two-dimensional development of a jet from a slit in a high-pressure reservoir. Each case presented tests the positioning of the DSMC patches and confirms proper resolution of wave phenomena.

In the hybrid simulations, test conditions indicate atmospheric density at 80-km altitude (18.46 mg/m^3) and a temperature of 500 K. The grids employ equi-sized ADV and DSMC cells whose dimensions are specified in multiples of the rest mean free path in the region at test conditions. DSMC hard sphere particles have the mass of nitrogen molecules. Solutions are advanced with time steps

measuring 1 μs (except where indicated) on a DEC Alpha 3000/700 workstation.

Nonadaptive Hybrid Calculations

Steady Shock

In this calculation DSMC captures a stationary Mach 3 shock wave while ADV computes the upstream and downstream regions. Figure 7 shows 70 overlaid independent realizations of the solution, each sampled 10 time steps apart.

Each of the 48 DSMC cells contains about 200 simulated molecules upstream and 600 downstream of the shock. DSMC ghost zones (10 cells wide, $n = 5$ levels per cell) provide smooth data to the adjacent ADV regions. Both DSMC and ADV cells measure 0.4 upstream rest mean free paths. Rankine–Hugoniot equations determine the initial profile. Subsequently, constant Mach 3 upstream flow is maintained at test conditions (defined earlier) while extrapolation of properties is imposed at the downstream boundary. Periodic boundary conditions are applied in the y direction. The simulation yields the correct shock shape. Figure 8 shows good agreement between the ensemble-averaged hybrid density profile (solid line) and the shock solution from Bird's DSMC1S code included in Ref. 4. The shock half-slope thickness spans approximately four upstream rest mean free paths.

The quieting effect of ghost cells on either side of the DSMC domain in Fig. 7 demonstrates the ability of the ghost cells to reduce statistical noise in the properties passed to ADV zones. The fivefold increase in ghost particles produces roughly the expected 60% noise reduction. Because the upstream flow is supersonic, noise propagation occurs only in the subsonic downstream ADV region.

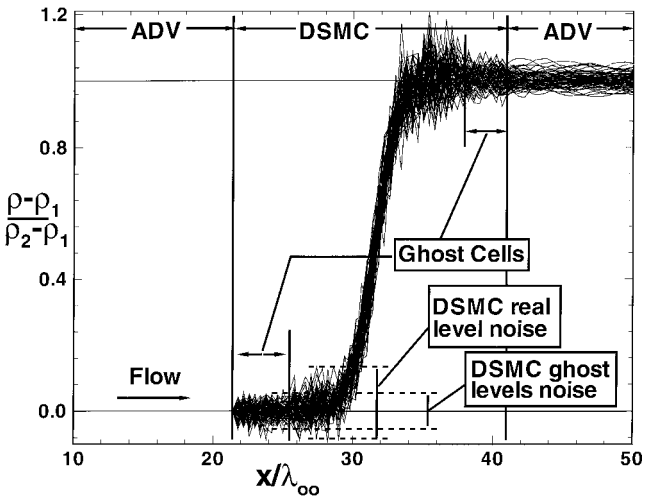

Fig. 7 Mach 3.0 standing shock.

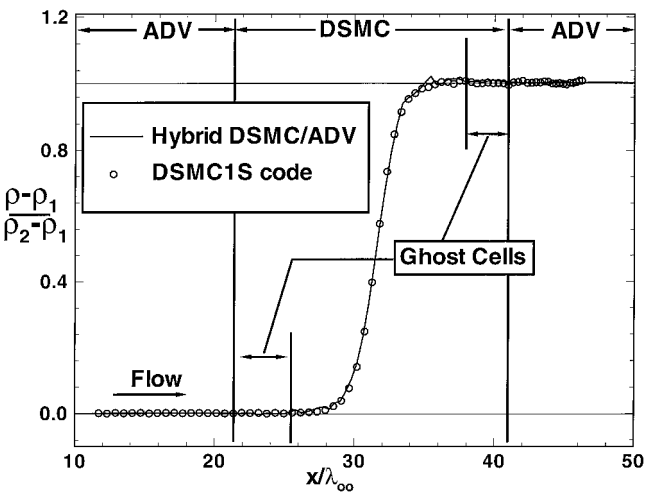

Fig. 8 Mach 3.0 standing shock: comparison with Bird's[4] DSMC code.

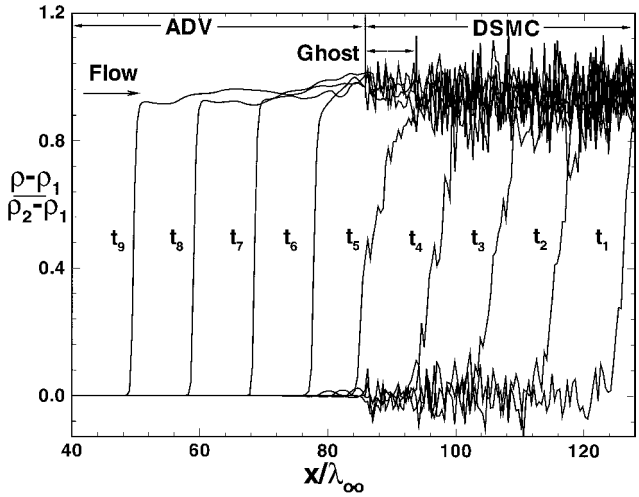

Fig. 9 Traveling normal shock wave.

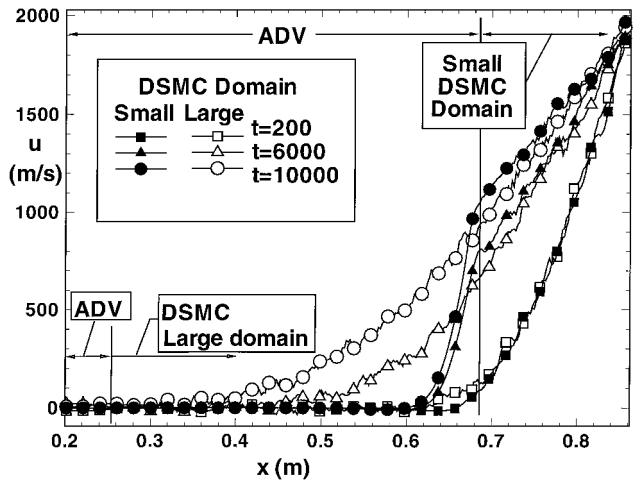

Fig. 10 Compressible Rayleigh problem.

Traveling Normal Shock Wave

Figure 9 shows nine successive density realizations of a normal shock wave passing through a stationary ADV–DSMC interface. Uniformly moving the flow toward the right-hand solid wall (at $x/\lambda_\infty \sim 128$) at 400 m/s generates a Mach 1.7 reflected shock wave. Constant upstream inflow is maintained at test conditions while periodic boundary conditions are applied in the y direction.

The whole domain consists of 105 DSMC cells adjacent to the specular wall on the right-hand side of the domain and 215 ADV cells to the left of the interface. The DSMC region near the ADV–DSMC interface comprises $n = 5$ levels of ghost cells, 20 cells wide. Each cell has 400 simulated molecules upstream of the shock. The computation was advanced through 900 time steps.

The shock thickness spans about eight rest mean free paths in the DSMC region, whereas in the ADV region it is thinned considerably (to about three cells) but has a finite thickness due to the effect of numerical viscosity. The solution yields the correct Rankine–Hugoniot density ratio for Mach 1.7. In the ghost cells the fivefold increase in ghost particles produces a clear reduction in noise.

Compressible Rayleigh Problem

The compressible Rayleigh problem consists of a flat plate suddenly moved in its own plane and is used to illustrate the nature of a shear layer passing through a fixed ADV–DSMC interface. Figure 10 shows tangential velocity profiles for this flow.

Two DSMC–ADV solutions with differing DSMC domains are presented. The whole domain consists of 400 cells. One computation (hollow symbols) uses 280 DSMC cells adjacent to the diffuse right-hand wall, whereas the second computation (solid symbols) uses only 80 DSMC cells. Both DSMC domains use 20 ghost cells, $n = 5$,

near the ADV–DSMC interface. Each DSMC cell is initialized with 200 simulated molecules. The solution is advanced through 10,000 time steps. Velocity profiles tangential to the plate are plotted after 200, 6000, and 10,000 steps.

Periodic boundary conditions are applied in the vertical direction, whereas in the horizontal direction extrapolation of flow properties is imposed at the left side of the ADV domain. The diffusely scattering plate ($T_w = T_\infty$) at the right side of the DSMC domain is suddenly moved upward in its own plane at 2000 m/s (Mach 4) at $t = 0$.

Following the downstream (left side) departure of initial weak shocks and rarefactions, the diffusively growing shear layer gradually penetrates the interface. At $t = 200$, before the layer crosses the small domain interface, the agreement between the two solutions is very good. As the shear layer crosses the small domain interface (starting at $\sim t = 200$), a slope discontinuity occurs because the choice of collision cross section determines the viscosity in the DSMC method, whereas only numerical viscosity affects the ADV result. The discontinuity in viscosity at the interface leads to thinning of the viscous shear region and a corresponding increase of the velocity gradient in the ADV. This example illustrates that the interface should remain within the nearly irrotational flow to avoid such errors. There is a small velocity slip adjacent to the wall. The large DSMC simulation captures the decay to the far-field value (near zero u and v velocity components) similar to that in the incompressible Rayleigh problem.

Supersonic Jet Flow Striking a Vertical Flat Plate

Figure 11 shows density contours from a two-dimensional calculation of supersonic jet flow impinging on a vertical flat plate.

Two separate DSMC patches, embedded in the ADV domain, contain the slit vertical walls and the target plate, respectively. The patches remain fixed throughout the calculation. The whole domain (320×168 cells) consists of 5324 DSMC cells (3920 pure DSMC cells and 1404 ghost DSMC cells) and 48,436 ADV cells. We model the slit with two vertical specularly reflecting walls on either side of a centered opening. The opening is 10.4 λ_∞ high (13 cells). The specularly reflecting target plate measures 10.4 λ_∞ high (13 cells) and is positioned 131.2 λ_∞ (164 cells) to the left of the slit. The simulation has a Reynolds number of about 200 based on the upstream speed of sound, the high-pressure reservoir density, and the slit height.

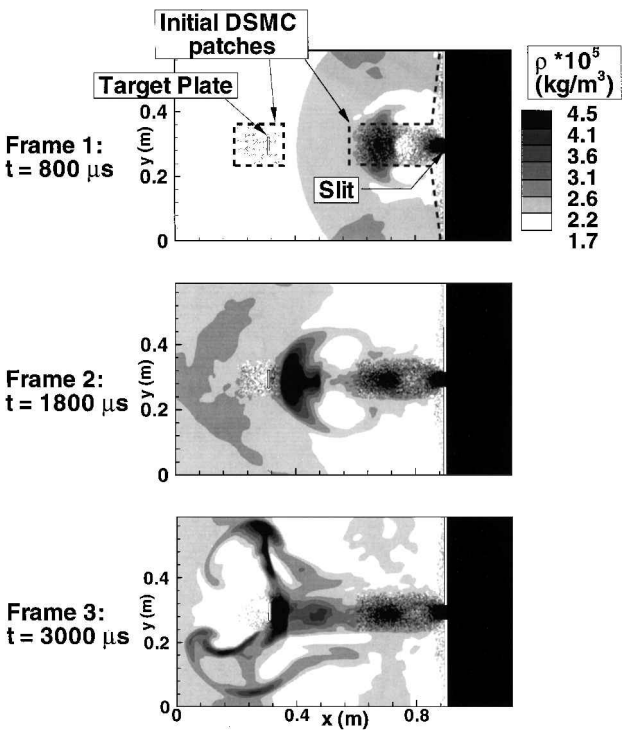

Fig. 11 Hybrid calculation of unsteady plume flow over a normal flat plate.

Periodic boundary conditions are applied in the vertical direction, whereas property extrapolation from the boundary cells is enforced in the horizontal direction. To create a starting pressure ratio of 10:1, we initialize the DSMC cells to the left of the slit with 20 simulated molecules and those to the right with 200 molecules. The solution is advanced toward a steady solution through 15 realizations of 200 time steps each. The flow develops from the initial state of rest and test conditions assigned to the low-pressure region.

Within the high-pressure reservoir, the ADV–DSMC interface adequately simulates subsonic inflow/outflow conditions at the right interface of the fixed DSMC patch that envelops the slit wall. Choked flow exists at the throat. Frame 1 shows the propagation of a weak initial shock wave (~Mach 1.3) and the resulting reflected shocks at the lower and upper boundaries. The initial weak shock wave has exited the downstream boundary in frame 2, which shows the jet structure just before it impinges on the vertical target plate. Notice the formation of two vortical structures of opposite sense on either sides of the jet. Frame 3 shows the jet impinging on the vertical flat plate and the formation of two additional counter-rotating vortices originating at the plate tips. The residual statistical noise in the DSMC calculation produces acoustic disturbances that propagate in the subsonic regions on both sides of the jet. Because of these propagating weak waves the jet does not impinge with its longitudinal axis exactly perpendicular to the target plate, which results in the asymmetric development of the plate tip vortices.

Density contours show the near jet region bounded in the vertical direction by shear layers (free boundaries). As seen in frame 3 the flow suddenly expands from the slit and is recompressed by a diffuse normal shock at $x \sim 0.76$ m. Subsequent expansion results in supersonic flow that causes the bow shock ahead of the vertical plate.

Adaptive Hybrid Calculations

One-Dimensional Shock Tube Problem

Figure 12 shows three realizations from a hybrid ADV–DSMC simulation of a one-dimensional shock tube along with results from a pure DSMC computation.

The simulation models an initial density ratio of 10 and an initial temperature ratio of 4. The driven section is at test conditions.

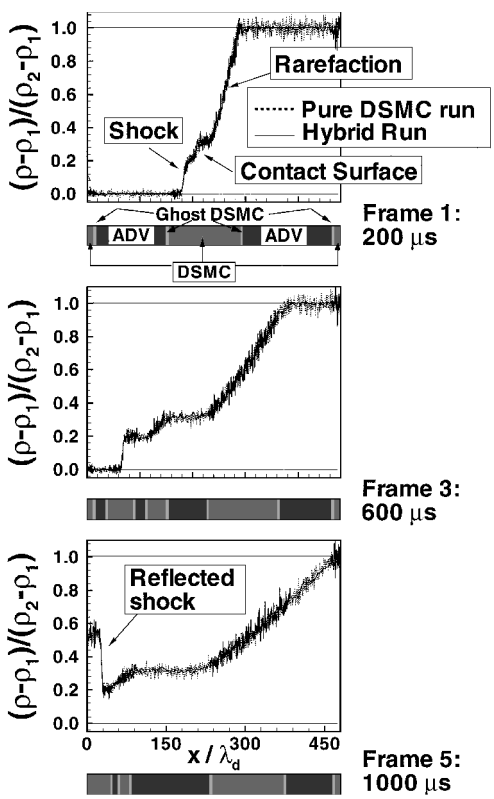

Fig. 12 Hybrid ADV–DSMC simulation of one-dimensional shock tube; gray-scale bar below each image indicates evolving DSMC and ADV patches.

Periodic boundary conditions are applied in the vertical direction. The whole domain consists of 960 equi-sized cells of length equal to 0.8 λ_d. Each DSMC cell in the driven section initially contains 100 particles in the full DSMC simulation and 50 particles in the hybrid simulation. Multiple DSMC patches evolve in time from a initial 100-cell DSMC patch that contains the initial density step profile. Each end of the DSMC patches has five ghost cells, $n = 5$.

The hybrid solution agrees well with the full DSMC calculation. The initial cell length of 0.8 λ_d leads to mild underresolution of the shocks because the local mean free path decreases as the flow is compressed. However, moving DSMC patches properly track the relevant unsteady gradients. Notice the formation of a strong shock wave as the leading shock rebounds from the wall just before it interacts with the contact surface.

Conclusion

A novel, strongly coupled, hybrid ADV–DSMC adaptive method was created and applied to one-dimensional and two-dimensional flows with encouraging results. The coupling was implemented through an interface that initializes ADV buffer cells with DSMC properties and uses DSMC reservoir cells to inject particles. The two methods exchange information at every time step allowing time-accurate treatment of unsteady flows. A novel approach to reduce the statistical noise propagating into continuum regions from the DSMC interface consists of using ghost regions surrounding DSMC patches. Simple ASCII grid maps permit the positioning and reshaping of DSMC patches in nonequilibrium flow areas through the use of cutoff thresholds for the breakdown parameters. The continuous coupling between ADV and DSMC at the interface and the adaptive DSMC patches offers an accurate and computationally efficient way to analyze unsteady flows that combine rarefied and continuum characteristics. The interface appears reasonably stable even in regions of stagnation flow. We finally note that such a hybrid approach is useful to create a subsonic inflow/outflow boundary condition for the DSMC approach.

Acknowledgments

This work was supported in part by NASA under the university grant program (Grant NAG9-804). Some of this material was first presented in modified form in AIAA Paper 97-1006, Jan. 1997. We would like to thank F. E. Lumpkin III, and G. J. LeBeau of NASA Johnson Space Center and J. V. Austin of the University of Texas at Austin for helpful discussions. Color pictures and animations of many of the results are also available.[§]

[§]The color pictures and animations may be found at the following Web site: http://www.ae.utexas.edu/~roberto/research.html.

References

[1]Anderson, D., Tannehill, J., and Pletcher, R., *Computational Fluid Mechanics and Heat Transfer*, 1st ed., Hemisphere, New York, 1984, pp. 235–246.

[2]Hirsch, C., *Numerical Computation of Internal and External Flows*, Vol. 2, Pt. 6, Wiley, New York, 1988.

[3]Bird, G. A., *Molecular Gas Dynamics and the Direct Simulation of Gas Flows*, Clarendon, Oxford, England, UK, 1994, Chaps. 11–16.

[4]Bird, G. A., "Monte-Carlo Simulation in an Engineering Context," *Rarefied Gas Dynamics,* edited by S. S. Fisher, Pt. 1, Vol. 74, Progress in Astronautics and Aeronautics, AIAA, New York, 1981, pp. 239–255.

[5]Lumpkin, F. E., III, Stuart, P. C., and LeBeau, G. J., "Enhanced Analyses of Plume Impingement During Shuttle-Mir Docking Using a Combined CFD and DSMC Methodology," AIAA Paper 96-1877, June 1996.

[6]Wilmoth, R. G., LeBeau, G. J., and Carlson, A. B., "DSMC Grid Methodologies for Computing Low-Density, Hypersonic Flows About Reusable Launch Vehicles," AIAA Paper 96-1812, June 1996.

[7]Hash, D. B., and Hassan, H. A., "A Decoupled DSMC/Navier-Stokes Analysis of Transitional Flow," AIAA Paper 96-0353, Jan. 1996.

[8]Hash, D. B., and Hassan, H. A., "Assessment of Schemes for Coupling Monte Carlo and Navier–Stokes Solution Methods," *Journal of Thermophysics and Heat Transfer*, Vol. 10, No. 2, 1996, pp. 242–249.

[9]Wadsworth, D. C., and Erwin, D. A., "One-Dimensional Hybrid Continuum/Particle Simulation Approach for Rarefied Hypersonic Flows," AIAA Paper 90-1690, June 1990.

[10]Wadsworth, D. C., and Erwin, D. A., "Two-Dimensional Hybrid Continuum/Particle Approach for Rarefied Hypersonic Flows," AIAA Paper 92-2975, July 1992.

[11]Golse, F., "Applications of the Boltzmann Equation Within the Context of Upper Atmosphere Vehicle Aerodynamics," *Computer Methods in Applied Mechanics and Engineering*, Vol. 75, Nos. 1–3, 1989, pp. 299–316.

[12]Hash, D. B., and Hassan, H. A., "Two Dimensional Coupling Issues of Hybrid DSMC/Navier–Stokes Solvers," AIAA Paper 97-2507, Jan.1997.

[13]Bird, G. A., "Breakdown of Translational and Rotational Equilibrium in Gaseous Expansion," *AIAA Journal*, Vol. 8, No. 11, 1970, pp. 1998–2003.

[14]Boyd, I. D., Chen, G., and Candler, G. V., "Predicting the Failure of the Continuum Fluid Equations in Transitional Hypersonic Flows," AIAA Paper 94-2352, June 1994.

[15]Nadiga, B. T., "An Euler Solver Based on Locally Adaptive Discrete Velocities," *Journal of Statistical Physics*, Vol. 81, Nos. 1–2, 1995, pp. 129–146.

[16]Nadiga, B. T., "An Adaptive Discrete Velocity Model for the Shallow Water Wave Equations," *Journal of Computational Physics*, Vol. 121, No. 2, 1995, pp. 271–280.

[17]Nadiga, B. T., and Pullin, D. I., "A Method for Near-Equilibrium Discrete-Velocity Gas Flows," *Journal of Computational Physics*, Vol. 112, No. 1, 1994, pp. 162–172.

[18]Chen, G., and Boyd, I. D., "Statistical Error Analysis for the Direct Simulation Monte Carlo Technique," *Journal of Computational Physics*, Vol. 126, No. 2, 1996, pp. 434–448.

[19]Guttman, I., Wilks, S. S., and Hunter, J. S., *Introductory Engineering Statistics*, 3rd ed., Wiley, New York, 1982, pp. 178, 179.

R. G. Wilmoth
Associate Editor